



Experimental limitations in impedance spectroscopy: Part IV. Electrode contact effects

Jin-Ha Hwang^a, K.S. Kirkpatrick^a, T.O. Mason^{a,*}, E.J. Garboczi^b

^aDepartment of Materials Science and Engineering, Northwestern University, Evanston, IL, 60208, USA

^bNational Institute of Standards and Technology, Building Materials Division, Gaithersburg, MD 20899, USA

Received 5 August 1996; accepted 10 January 1997

Abstract

A 'spreading resistance' contact between electrode and specimen can increase or even dominate the apparent bulk resistance of an electroceramic specimen. For true point contacts, a single arc will appear in impedance spectra, whose diameter is essentially the spreading resistance due to the contact and whose time constant is identical to that of the bulk, but with a correspondingly smaller capacitance. When a planar electrode with multiple point contacts is involved, a separate electrode arc occurs whose diameter is due to spreading resistance, but whose capacitance tends to be dominated by the 'air gap' capacitance between the electrode and the rough surface of the ceramic. In this study impedance spectroscopy was employed to study the effects of temperature, oxygen partial pressure, and mechanical loading on the contact impedance of gold electrodes on nanophase cerium dioxide. Results were confirmed by pixel-based computer simulations.

Keywords: Impedance spectroscopy; Point contact; Contact impedance

1. Introduction

Impedance spectroscopy (IS) is a powerful technique to resolve bulk versus interfacial electrical properties in electroceramics, to study interfacial phenomena in batteries and fuel cells, and to monitor the corrosion of metals in aqueous environments. The monograph of Macdonald provides an excellent introduction to these subjects [1]. Unfortunately, there are a number of experimental limitations which must be overcome to obtain reliable IS data. In the prior papers of this series we have addressed the influence of high impedance reference electrodes

[2,3] and the placement/geometry of the reference electrode [4] on the reliability of three-point IS measurements in materials studies. In the present work we address the role of spreading resistance contacts at noble metal electrodes (Au) in the impedance spectra of electroceramics (e.g., nanophase ceria). Various remediation strategies are also discussed.

An early treatment of spreading resistance can be found in the monograph of Holm [5]. A more thorough development was published by Newman [6]. For a circular contact of infinite conductivity on the surface of a resistive specimen, the contact resistance (R_c) is given by:

$$R_c = (4a\sigma)^{-1}, \quad (1)$$

*Corresponding author. Tel.: +1 847 491 3198; fax: +1 847 491 7820; e-mail: t-mason@nwu.edu

where σ is the conductivity of the specimen and a is the radius of the contact. This resistance arises due to current spreading within the specimen in the vicinity of the contact and is dependent only on the radius of the point contact, i.e., it is independent of the dimensions of the sample as long as they are substantially larger than the contact radius. As we will show, this resistance is distinct from and adds to the geometric resistance (R_s) of the specimen:

$$R_s = \sigma^{-1} (l/A), \quad (2)$$

where l and A are length and cross-sectional area, respectively. Hence, one means to establish whether spreading resistance effects are present is to test whether the resistance being measured changes linearly ($R_s \gg R_c$) or not significantly ($R_c \gg R_s$) with the sample dimensions. Ultimately, as shown below, the best means to establish the presence of spreading resistance effects in two-point IS measurements is to perform simultaneous four-point DC resistivity measurements. The true DC resistance should always agree with R_s , whereas the apparent bulk resistance in two-point IS will be the sum of R_s and R_c , as we will show.

IS allows both resistance and capacitance to be obtained from a given arc or semicircle in a Nyquist plot of $-\text{imaginary impedance } (-\text{Im}(Z))$ versus real impedance ($\text{Re}(Z)$), as in Fig. 1c. This spectrum results from the equivalent circuit in Fig. 1a, where R_s is the sample resistance and C_s is the sample capacitance:

$$C_s = \epsilon \epsilon_0 (A/l). \quad (3)$$

Here ϵ is the relative dielectric constant, ϵ_0 is the permittivity of free space, and the geometric parameters are as defined above. The frequency at the top of the arc (ν_{top}) is given by [1]:

$$\nu_{\text{top}} = (2\pi R_s C_s)^{-1}. \quad (4)$$

(For the sake of simplicity, we will neglect any dispersion of time constants due to heterogeneities within the sample that would lead to depression of the arc below the real axis.)

The point contact capacitance associated with a circular electrode of infinite conductivity and radius, a , placed on a large sample is given by [7,8]:

$$C_c = 4a\epsilon\epsilon_0, \quad (5)$$

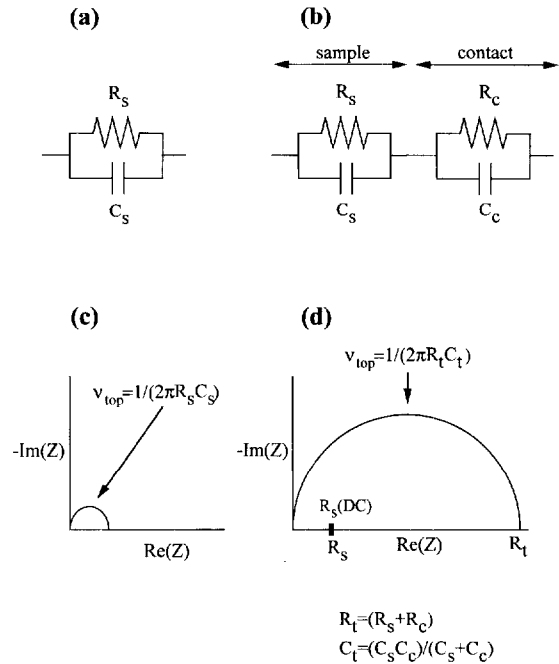


Fig. 1. Equivalent circuit models (a) w/o and (b) w/ contact effect at the specimen/electrode interface. The corresponding impedance spectra, (c) and (d).

where ϵ and ϵ_0 are as defined above. Fig. 1d shows the calculated Nyquist plot for a sample with $R_c = 5R_s$. Because the time constant (RC) is identical for the two processes:

$$RC = R_s C_s = R_c C_c = \sigma^{-1} \epsilon \epsilon_0 \quad (6)$$

(both processes occur in the bulk of the specimen), only one arc is obtained whose diameter is the sum of R_s and R_c . The frequency at the top of this arc is given by

$$\nu_{\text{top}} = (2\pi R_t C_t)^{-1} \quad (7)$$

where $R_t = R_s + R_c$ and $C_t = (C_s C_c) / (C_s + C_c)$. The characteristic frequency, ν_{top} , is identical to that of the bulk response in Fig. 1c, due to the equality of time constants in Eq. (6). This means that it is impossible to discriminate bulk and spreading resistance contributions due to point contacts by two-point IS. The only means to test for the presence of a spreading resistance effect is to determine the true

sample resistance by simultaneous four-point DC resistivity measurements. In Fig. 1c the arc radius (R_c) agrees with R_s (DC) whereas in Fig. 1d, the arc radius ($R_s + R_c$) is much larger than R_s (DC).

It is important to note that whereas R_c is inversely proportional to a (Eq. (1)), C_c is directly proportional to a (Eq. (5)). Therefore as a is decreased, point contacts produce large apparent resistances, but relatively small capacitances. When C_c is reduced below the level of the 'air gap' capacitance (see below) or the intrinsic apparatus capacitance (i.e., the capacitance measured at open-circuit), the spreading resistance contribution will reflect the larger capacitance and may develop a distinct arc of its own. This behavior is discussed further below.

There are numerous reports of resistance and/or impedance contributions attributed to interfaces in electroceramic systems. Some recent examples include Fletcher et al. [9], who reported interface impedance effects in yttria-stabilized zirconia (YSZ)/yttrium barium oxide (YBC) contacts. Kenjo and Nakagawa [10] attributed an ohmic resistance to electrode/electrolyte interfaces in systems based on YSZ. Fleig and Maier [11] attributed the impedance behavior of electrode/solid electrolyte interfaces to point contacts and a 'gap' capacitance (see below). It should be stressed that these effects were strictly geometric and ohmic and were in no way associated with electrochemical reactions or polarization effects.

The present work reports experimental and computer-simulated impedance spectra for an electroceramic (nanophase ceria) with what we interpret to be spreading resistance contributions at Au electrode contacts. This interpretation is confirmed by a variety of tests, including mechanical loading, temperature variations, and changes in the oxygen partial pressure. Four-point DC measurements are used throughout to confirm the true sample resistance in each case. The origins of and remedies for spreading resistance effects are also discussed.

2. Experimental

Nanophase cerium dioxide was obtained from Nanophase Technologies (Burr Ridge, IL). A specimen was uniaxially pressed into pellets (19 mm

diameter, 2.1 mm thick) at a pressure of 125 MPa, followed by cold isostatic pressing at 280 MPa. The compacted specimen was dried at 200°C for 2 h, in order to remove moisture, and presintered at 700°C/1 hour to approximately 70% theoretical density and a mean particle size of ~15 nm, confirmed by field emission scanning electron microscopy. From this pellet, IS specimens (2.1 mm × 1.9 mm × 0.7 mm) and conductivity bars (1.7 mm × 1.5 mm × 8.5 mm) were cut with diamond saw. The surfaces of the impedance specimens were subsequently abraded with 600 grit SiC paper followed by diamond polishing with 30 μm, 6 μm, and 1 μm diamond pastes, using a specially designed stainless steel polishing fixture, in order to provide even polishing and parallel surfaces. When an intentionally roughened surface was required, one side of a specimen was abraded with 400-grit SiC paper.

Some of the samples were sintered at 1100°C for 1 h to nearly full density and large grain size (~μm). These specimens exhibited a grain boundary arc separate from the bulk response and were employed to study contact effects when a larger capacitance feature is present.

Contacts to impedance specimens were made directly, i.e., by pressing the surface against gold foil, or by first depositing a 0.15 μm thick layer of gold by sputtering. Gold was chosen as its work function is virtually identical to that of cerium dioxide [12–14] and should therefore provide ohmic contacts. DC conductivity specimens were similarly electroded (two-point square specimens) or, as four-point bars, were pressed between gold foil current leads. Tight loops of gold wire, wrapped around these bars at ~1/3 and ~2/3 positions along the length of the bars, served as voltage leads.

Impedance spectra were collected using an HP-4192A low-frequency impedance analyzer (Hewlett Packard, Palo Alto, California). In the absence of electrode polarization features at low frequencies (electronic conduction predominates), a large oscillating amplitude could be employed (1 V) with no apparent nonlinearities. The spectra were acquired in a logarithmic manner between 11 MHz and 5 Hz with 20 points per decade. The collected spectra were null-corrected for unwanted apparatus contributions using the open-circuit/short-circuit procedure described previously [15]. Equivalent circuit fitting

of the experimental spectra was carried out using a commercially available software package [16].

Two- and four-point DC resistivity measurements were performed using a Keithley 220 current source and a Keithley 196 digital multimeter (Keithley Instruments, Inc., Cleveland, Ohio). A standard current-reversal procedure was employed to remove unwanted voltage effects, such as thermal e.m.f.s, in DC resistivity measurements. Electrical measurements were made between 350° and 550°C in a controlled atmosphere muffle furnace. In order to compare two-point impedance spectra with the four-point DC resistivity, two specimen holders were bound together and placed in the same temperature zone. By taking into account the differences in geometry, a comparable DC resistance could be calculated for the impedance samples on the basis of the four-point bar samples. The temperature was controlled within $\pm 1^\circ\text{C}$ by using a Eurotherm programmable controller (Model 826 Eurotherm Co., Reston, Virginia). Oxygen partial pressure was controlled between 1 and 10^{-3} atm, using premixed Ar/O₂ mixtures. The precise oxygen partial pressure was determined with an oxygen sensor.

Computer simulations of impedance spectra were performed using a pixel-based model [17–20]. A 3-D digital image was generated, where each pixel is a cube, as described below. The complex conduction equation, essentially Laplace's equation, must then be solved for this geometry. Using the finite element method [21] a node is placed at each corner, each pixel being treated as a tri-linear finite element,

and the resulting linear equations are then solved. Alternatively, nodes can be placed in the middle of each pixel and Laplace's equations can be discretized using finite difference methods. Both approaches work equally well. For this work the finite difference method was used to solve for the complex conductivity of the model sample. The linear equations resulting from the discretization were solved using a conjugate gradient relaxation method [22]. Each pixel is a node in a three-dimensional network consisting of appropriate resistors and capacitors representing the appropriate 'phase,' i.e., ceria, gold, or air. The parameters were chosen to reflect the values obtained experimentally. To simulate surface roughness, an idealized ridge structure was constructed as in Fig. 2. Each pixel is 6.9 μm on a side such that ridges 13.8 μm wide and spaced every 13.8 μm extend into the plane of the figure. (Note: for comparison, a grit size of 400 corresponds to a mean abrasive particle size of 20–23 μm .) None of these ridges is in contact with the electrode, however. Contact is made only every 20th ridge, these being an additional pixel length in height. This simulates the random roughness of the real surface, so that the flat electrode would only touch some of the ridges. The size of the unit cell of the model was $(x, y, z) = (80, 2, 100)$ pixels, with periodicity in the x and y directions. It should be stressed that the structure in Fig. 2 is only an idealized representation, designed to qualitatively have some of the features of the real system. The actual surface and contact situation is expected to be much more complicated.

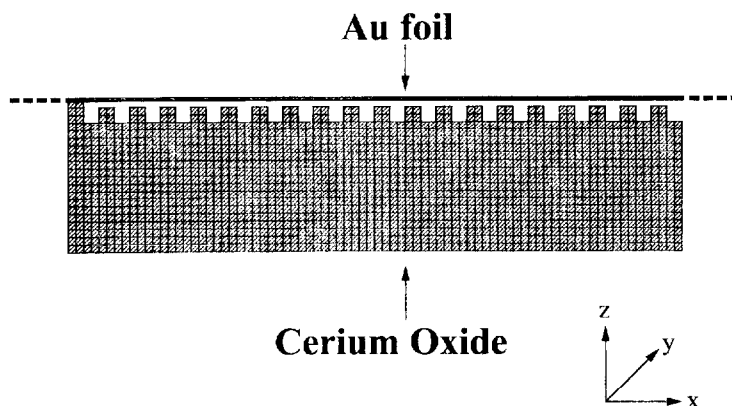


Fig. 2. Schematic diagram of the electrode condition at the specimen/electrode interface for pixel-based computer modeling.

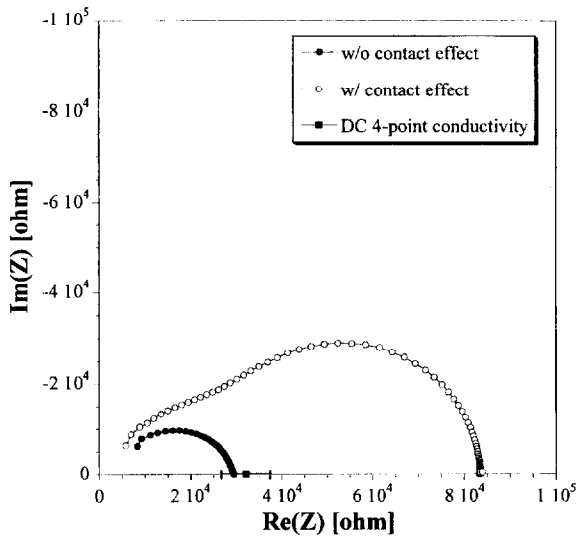


Fig. 3. Impedance spectra at 550°C in air without (w/o) contact effect and with (w/) contact effect versus the resistance from 4-point DC conductivity measurement.

3. Results and discussion

Fig. 3 compares the impedance spectra for two samples at 550°C in air. Each was pressed between gold foils, however the one marked 'w/o contact effect' had both surfaces polished to 1 μm and 0.15 μm layers of gold deposited on them. The other specimen marked 'w/ contact effect' had the same treatment (1 μm polishing plus gold deposition) on only one surface. The other surface was abraded with 400 grit paper and had no gold deposited on it. For comparison, the resistance calculated from the companion four-point DC resistivity bar is also shown on the real impedance axis. As can be seen, the low frequency (right side) intercept of the single arc for the polished and electroded specimen agrees well with the true DC resistance. In contrast, the sample whose abraded surface was merely pressed against the gold foil has a much higher low frequency (right side) intercept. Furthermore, there are now two discernible arcs in the impedance spectrum. It should be noted that this is strictly an electrode artifact. When the abraded surface was appropriately polished and gold-coated, single-arc behavior in agreement with DC resistance could be restored. Although Schottky barriers are not anticipated in this system,

due to the similarity of work functions, current–voltage tests were conducted to check for nonlinearity. In every instance ohmicity was confirmed.

Mechanical loading tests were carried out at 550°C to see how the impedance of the sample with the abraded/pressed electrode would change with pressure. A simple screw and spring device was used to gradually increase the pressure on the electrode/sample without fracturing the specimen. Although precise pressure measurements were not made, Fig. 4 shows a steady decline in overall resistance (low frequency, rightmost, intercept) as pressure increases, largely associated with a decrease in the low frequency arc. It should also be observed that a true sample-only response (a single arc whose resistance is the same as the DC resistance) could not be obtained. While the resistance of the low frequency (rightmost) arc decreased by almost a factor of 3, the capacitance of this arc remained virtually constant. This is attributable to the 'air gap' capacitance, discussed further below.

The specimen 'w/ contact effect' (Fig. 3) having one roughened/pressed contact and one polished/electroded contact was also subjected to IS measurements at 500°C over a range of oxygen partial pressures (0.1% to 100% oxygen). The impedance

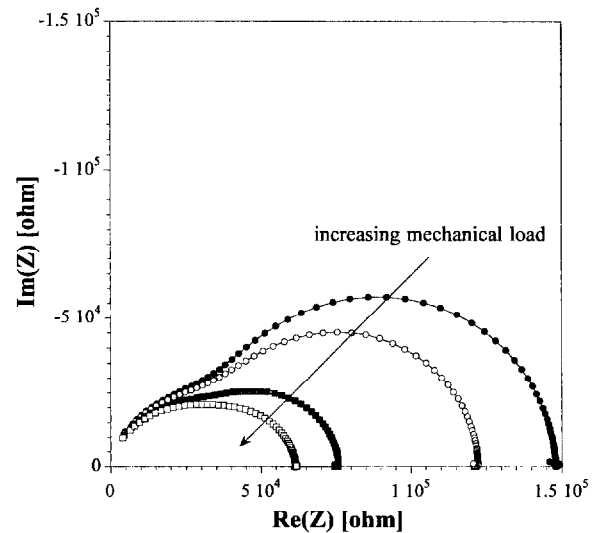


Fig. 4. The variation of impedance spectra with the mechanical load applied for a sample with a poor specimen/electrode contact. ($T=550^{\circ}\text{C}$ in air).

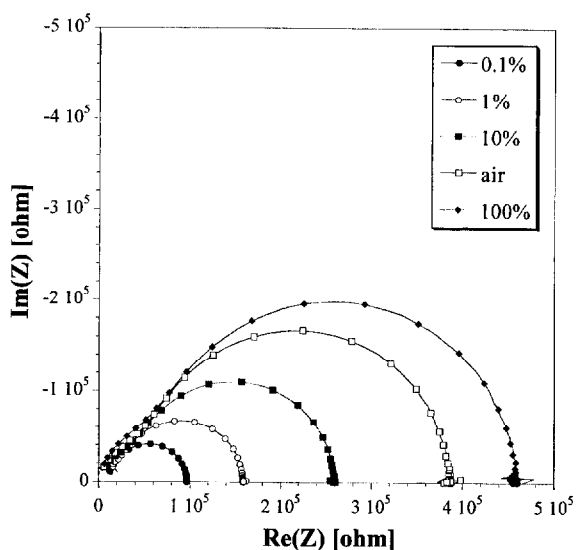


Fig. 5. Impedance spectra at 500°C as a function of oxygen partial pressure for a sample with a poor specimen/electrode contact.

data at 500°C versus P_{O_2} are displayed in Fig. 5. These spectra could be deconvoluted into two separate arcs, both of which vary with P_{O_2} . Based upon the mechanical loading results, we have identified the low frequency (rightmost) arc with the contact effect. The inverse resistances of each arc are plotted versus P_{O_2} in the log–log plot of Fig. 6. The slopes, which can be attributed to underlying point defect mechanism(s) [23], are virtually identical. Similar impedance spectra were obtained for different temperatures in air (not shown). Again, two distinct arc contributions could be resolved, both of which varied with temperature. The inverse resistances of each arc (log scale) are plotted versus inverse temperature in Fig. 7. The slopes, attributable to the same activated processes [23], are again virtually identical. In no instance did the capacitance of the contact arc change significantly with P_{O_2} or T .

The agreement in P_{O_2} - and T -dependencies between the contact and bulk features in Figs. 6 and 7 is experimental evidence for a spreading resistance effect. For a point contact the ratio of R_s (Eq. (2)) and R_c (Eq. (1)) will be:

$$R_s/R_c = (4al)/A, \quad (8)$$

which should be constant as long as the geometry of

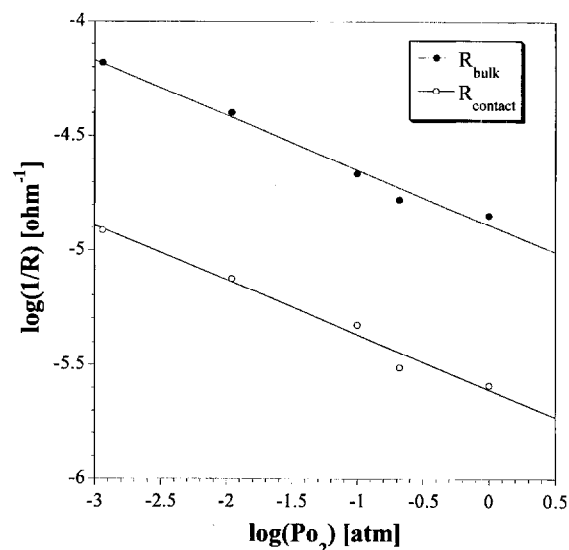


Fig. 6. Oxygen partial pressure dependence of the bulk and contact resistances for a sample with a poor specimen/electrode contact. ($T=500^\circ\text{C}$.)

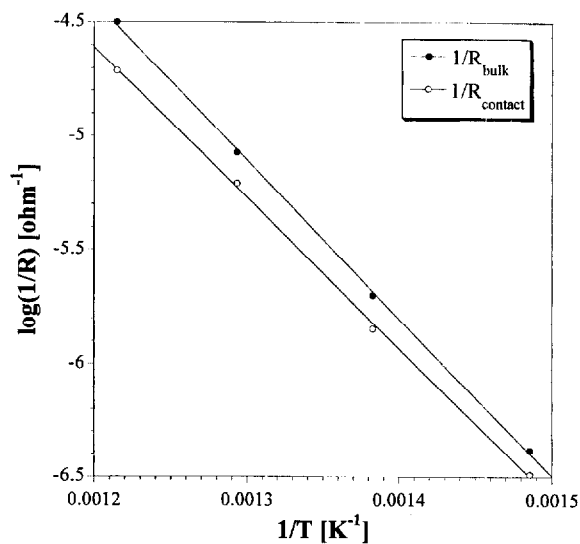


Fig. 7. Temperature dependence in air of the bulk and contact resistances for a sample with a poor specimen/electrode contact.

the sample (l/A) and the geometry of the contact (a) do not change with P_{O_2} or T . There are undoubtedly multiple point contacts involved in the present measurements. As long as the inter-contact distance is large relative to the radii of the contacts, Holm [5] has shown that:

$$R_c = (4 \sum a \sigma)^{-1}, \tag{9}$$

where $\sum a$ is the sum of the radii of the individual contacts. He has also developed more complicated formulae for when contacts are close enough to each other to ‘deflect’ the lines of flow associated with an adjacent contact. In any case, for a fixed geometry (i.e., the number, size, shape, and spacing of contacts) the ratio of R_s -to- R_c should remain constant.

The equation for contact capacitance corresponding to Eq. (9) would be:

$$C_c = 4 \sum a \epsilon \epsilon_0. \tag{10}$$

It follows that when R_c is a factor of 2 or 3 times larger than R_s (see Figs. 3 and 4), C_c should be the same factor smaller than C_s . Experimentally, a larger capacitance is obtained. Fig. 8 plots the real component of capacitance versus frequency corresponding to the impedance spectra in Fig. 5 (versus P_{O_2}). Two plateaus are seen at high and low frequency. The individual capacitance values can be obtained by modulus mode fitting [1]. The high frequency capacitance of 0.9 pF is in agreement with the bulk dielectric constant of ceria and the geometry of the specimen. The low frequency capacitance is similarly independent of experimental conditions, but

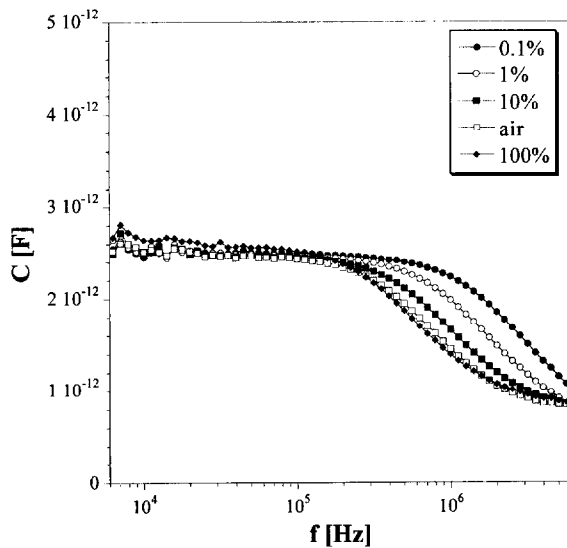
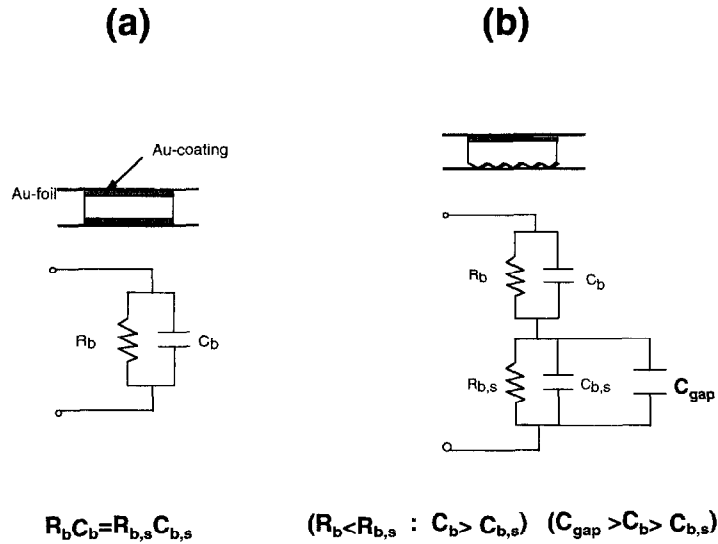


Fig. 8. Capacitance versus frequency at different oxygen partial pressures for a sample with a poor specimen/electrode contact. ($T=500^\circ\text{C}$.)

has a larger value of 3.9 pF. We agree with Fleig and Maier [11] that this capacitance is attributable to the gap between a planar electrode and the irregular surface of the sample. The schematic diagrams and equivalent circuits in Fig. 9 illustrate the difference between the polished/electroded specimen (Fig. 9a) and the roughened/pressed specimen (Fig. 9b). There are no spreading resistance/capacitance or ‘gap’ capacitance contributions in the polished/electroded specimen, so only the bulk arc is obtained (see Fig. 3). For the roughened/pressed specimen there is a spreading resistance ($R_{b,s}$) in series with the bulk elements. There should also be a small spreading capacitance ($C_{b,s}$), however this is overwhelmed by the gap capacitance in parallel with it (C_{gap}). A crude approximation of the ‘gap’ can be obtained using Eq. (3), the electrode area ($2.1 \text{ mm} \times 1.9 \text{ mm}$), the dielectric constant of air (1), and the experimental capacitance ($\sim 3.9 \text{ pF}$). The value obtained is $\sim 10 \mu\text{m}$, which is on the order of the size of abrasive grains used to roughen the surface.

In Fig. 10, the pixel-based model of Fig. 2 was used to simulate the impedance behavior without a spreading resistance effect, with spreading resistance but no ‘gap’ capacitance, and with spreading resistance plus a ‘gap’ capacitance. The ‘w/o contact’ (no spreading resistance) situation involved direct contact of the electrode to every surface pixel in Fig. 2 without surface roughness. A single arc is obtained, as in Fig. 3, using parameters consistent with the bulk resistance and dielectric constant of cerium dioxide (shown in Table 1). To approximate surface roughness, the model incorporated parallel ridges $13.8 \mu\text{m} \times 13.8 \mu\text{m}$ and separated by $13.8 \mu\text{m}$ along the surface, but not in contact with the electrode. Every 20th ridge was an additional pixel ($6.9 \mu\text{m}$) higher and in contact with the electrode. The relative dielectric constant of the ‘gap’ pixels could be set to zero (no gap capacitance) or unity (for gas or vacuum). As predicted in the Introduction, the impedance spectrum ‘w/ contact effect and w/o air gap capacitance’ ($\epsilon=0$) consists of a single arc, the diameter of which is approximately three times, and whose capacitance is approximately 1/3, that of the ‘no spreading resistance’ case, respectively. Since the pixel-based surface is only an idealized representation of the real surface, the equivalent value of R_c does not exactly



b: bulk

Fig. 9. Equivalent circuit models (a) w/o and (b) w/ poor contacts between the specimen and electrode for grain interior-controlled systems.

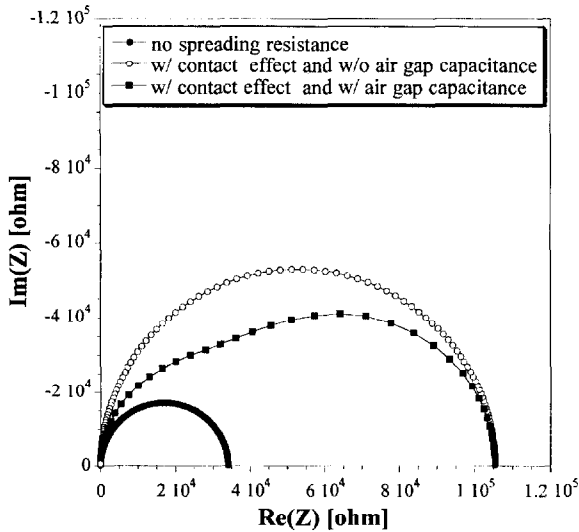


Fig. 10. Computer-based impedance spectra, including the bulk response only ('no spreading resistance'), with contact effect but no air gap capacitance, and with contact effect plus air gap capacitance.

match the experimental value in Fig. 3. When the 'gap' pixels are set to $\epsilon=1$, two separate arcs are obtained, again using parameters consistent with the

Table 1

Typical parameters for pixel-based computer modeling (of grain interior-controlled systems)

σ_b	5×10^{-5} (ohm ⁻¹ cm ⁻¹)
ϵ_b	30
ϵ_{air}	1
A/l	0.59 cm

experimental values in Table 1. Except for the slight evidence of arc-depression in Fig. 3 which is not reflected in Fig. 10 (pure capacitances were used in the simulations), the appearance of the two 'w/ contact effect' spectra is quite similar, but only when a 'gap' capacitance is taken into account. Furthermore, the capacitance obtained from fitting the low frequency arc using [16] is comparable to that obtained from fitting the same feature in Fig. 3, both of which are consistent with the scale of the surface roughness involved.

Until now, we have been dealing with sample and spreading resistance capacitances which are similar to or smaller than the 'gap' capacitance. In large-grained electroceramics it is possible to achieve substantially larger sample capacitances by virtue of a grain boundary effect. This arises when thin,

continuous, and more resistive grain boundary layers isolate each grain in what is commonly referred to as a ‘brick layer’ structure [1]. If bulk (grain interior) capacitance is in the pF range, grain boundary capacitance can be in the nF range. The equivalent circuit situations for the two cases above (‘w/o and w/ contact effect’), but with an additional grain boundary contribution in the sample, are shown in Fig. 11. Here the ‘gap’ capacitance is in parallel with both grain interior and grain boundary spreading resistance components (see the inset diagram). As discussed above, C_{gap} (~pF) is typically larger than the grain interior spreading capacitance ($C_{gi,s}$ ~0.3 pF – see Table 2), however it can be substantially smaller than the grain boundary spreading capacitance. (e.g., $C_{gb,s}$ ~50 pF in Table 2.)

‘Equivalent Circuit’ [16] was used to simulate the behavior of samples having both grain boundary and grain interior bulk contributions, with and without spreading resistance effects. Circuit elements were chosen to be consistent with the experimental values in Table 2 (see below). Once again, for simplicity, perfect capacitors were assumed (no arc depression). Typical results are shown in Fig. 12a and b, with

Table 2

Typical parameters for simulation of impedance spectra in systems controlled by grain interiors and grain boundaries using ‘Equivalent Circuit’ [16]

	w/ contact effect	w/o contact effect
R_{gi}	1×10^5 ohm	1×10^5 ohm
C_{gi}	1×10^{-12} F	1×10^{-12} F
$R_{gi,s}$	–	4×10^5 ohm
$C_{gi,s}$	–	2.5×10^{-13} F
R_{gb}	1×10^6 ohm	1×10^6 ohm
C_{gb}	2×10^{-10} F	2×10^{-10} F
$R_{gb,s}$	–	4×10^6 ohm
$C_{gb,s}$	–	5×10^{-11} F
C_{gap}	–	3×10^{-12} F

Fig. 12b magnifying the high frequency features. There are two perfect arcs in the ‘w/o contact effect’ case (closed circles). The large, low frequency arc has the resistance and capacitance of the grain boundaries (R_{gb} , C_{gb}) and the smaller, high frequency arc has the resistance and capacitance of the grain interiors (R_{gi} , C_{gi}). Things become considerably more complicated when a spreading resistance effect is involved (open circles). Here the smaller (left) of the two arcs is clearly a superposition of two

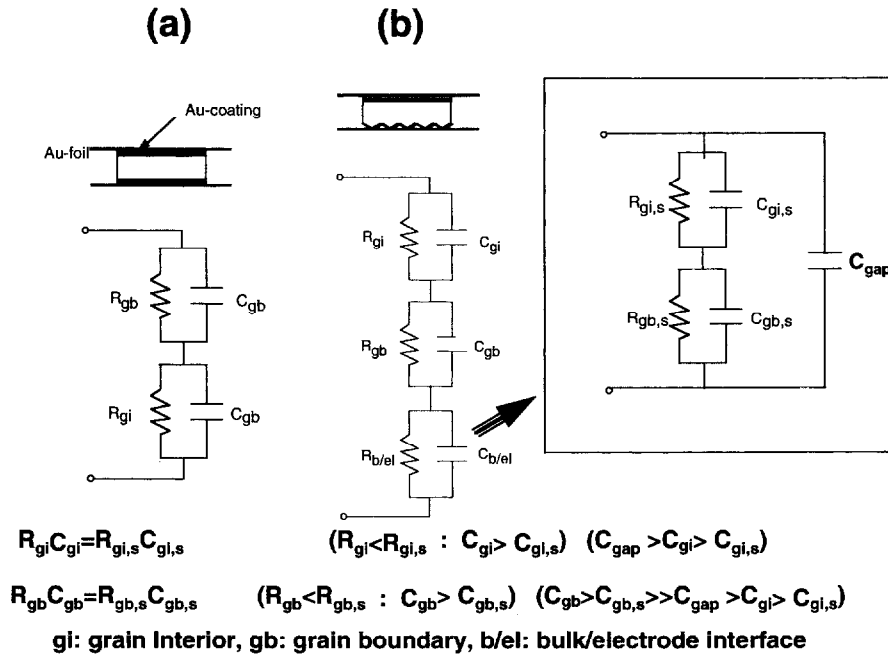


Fig. 11. Equivalent circuit models for the systems where the grain boundary response is added to the grain interior response.

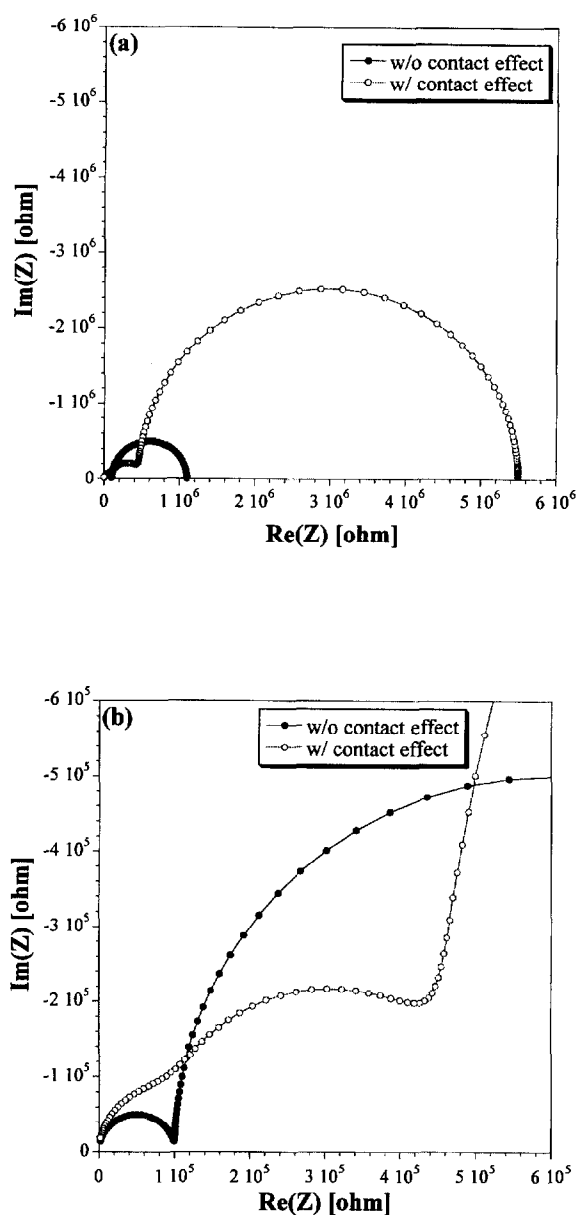


Fig. 12. (a) Simulated impedance spectra in grain boundary-controlled systems w/o and w/ contact effect, (b) enlargement of (a). (See Table 2 for parameters employed.)

individual arcs (see Fig. 12b). On the left is the grain interior contribution (R_{gi}) and on the right is the grain interior spreading resistance contribution ($R_{gi,s}$) – as per Table 2. The capacitances here involve a combination of the gap capacitance (C_{gap}) and the

grain interior capacitance (C_{gi}), since these are similar (see Table 2). The grain interior spreading capacitance, being an order of magnitude smaller, is insignificant. The rightmost, low frequency feature in Fig. 12a (open circles) is a single arc whose diameter is essentially $(R_{gb} + R_{gb,s})$ and whose capacitance is approximately $C_{gb}C_{gb,s}/(C_{gb} + C_{gb,s})$. The gap capacitance has little, if any, effect on this feature.

Fig. 13 displays the experimental results for dense, large-grained, ceria with one surface polished/electroded (Au) and the other roughened (400 grit) and pressed against gold foil to achieve an intentional spreading resistance effect. As above, Fig. 13a shows the extended spectrum whereas Fig. 13b magnifies the high frequency features. Except for slight arc depression in the experimental data, the appearance is in acceptable agreement with the equivalent circuit models of Fig. 12.

4. Conclusions

A widely held tenet in impedance spectroscopy is that two-point measurements allow for the separation of bulk response from electrode contributions. This is correct if there is no spreading resistance effect. The insidious aspect of spreading resistance contributions is that an electrode-related artifact shows up in the bulk arc, which can be significantly modified or distorted thereby. Bulk-like time constants are obtained. The low frequency intercept no longer represents the true DC resistance of the sample. Furthermore, an additional arc can be generated if a ‘gap’ capacitance is involved. In certain instances, the resulting two-arc behavior can be mistakenly interpreted as corresponding to grain interior and grain boundary contributions. In fact, both arcs are attributable to grain interiors – one from the bulk and one from spreading resistance near contacts.

There are a number of remedies for spreading resistance effects in impedance measurements. As pointed out previously, sample resistance should scale with sample geometry, whereas spreading resistance (for a given contact geometry) should be independent of sample geometry. For example, Fletcher et al. [9] showed that interface impedances with bulk-like time constants in YSZ/YBC heterocontacts and YSZ/YSZ homocontacts were independent of

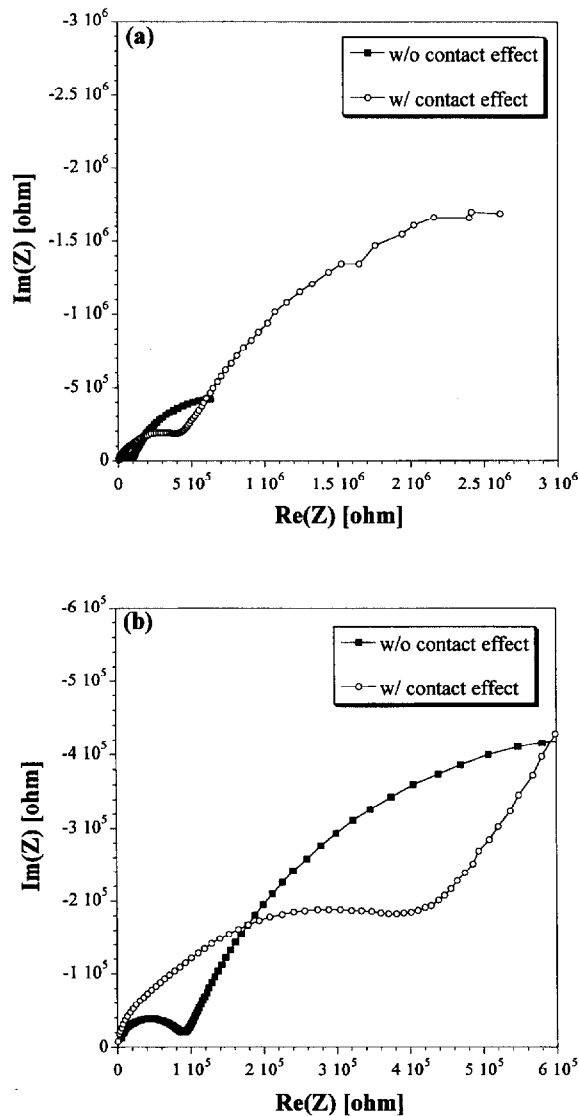


Fig. 13. Experimental impedance spectra at 550°C in air (a) w/o and (b) w/ contact effect for systems with grain interior- and grain boundary-controlled responses.

sample length. This is certain indication of a spreading resistance effect. Maintaining or reproducing a fixed contact geometry from sample-to-sample is difficult to achieve, however. An easier alternative is to make simultaneous four-point DC resistivity measurements on every specimen. If the low frequency intercept of the bulk feature agrees with the true DC resistance, spreading resistance can be neglected.

Careful attention to polishing and electroding is the best means to avoid spreading resistance contributions. In the present work, poor contact (i.e., spreading resistance) was obtained on poorly polished specimens with pressed metal electrodes. Good contact was achieved (no spreading resistance contributions) only when samples were finely polished and adequately electroded by sputtering.

Acknowledgments

This work was supported by the U.S. Department of Energy under grant no. FG02-84-ER45097 and made use of facilities of the Northwestern University Materials Research Center under grant no. DMR-91-20521.

References

- [1] J.R. Macdonald, *Impedance Spectroscopy*, Wiley, New York, 1987.
- [2] G. Hsieh, S.J. Ford, T.O. Mason, L.R. Pederson, *Solid State Ionics* 91 (1996) 191.
- [3] G. Hsieh, T.O. Mason, L.R. Pederson, *Solid State Ionics* 91 (1996) 203.
- [4] G. Hsieh, T.O. Mason, E.J. Garboczi, L.R. Pederson, *Solid State Ionics* 96 (1996) 153.
- [5] R. Holm, *Electric Contacts: Theory and Application*, Springer-Verlag, New York, 1967.
- [6] J. Newman, *J. Electrochem. Soc.* 113 (1966) 501.
- [7] W.R. Smythe, *Static and Dynamic Electricity*, McGraw-Hill, New York, 1950, p. 25.
- [8] J. Newman, private communication.
- [9] J.G. Fletcher, A.R. West, T.S. Irvine, *J. Electrochem. Soc.* 142 (1995) 2650.
- [10] T. Kenjo, T. Nakagawa, *J. Electrochem. Soc.* 143 (1996) L92.
- [11] J. Fleig, J. Maier, *Electrochimica Acta* 41 (1996) 1003.
- [12] A. Pfau, K.D. Schierbaum, W. Gopel, *Surface Science* 331–333 (1995) 1479.
- [13] R.E. Hummel, *Electronic Properties of Materials*, Springer-Verlag, New York, 1985, p. 306.
- [14] L.A. Azaroff, J.J. Brophy, *Electronic Processes in Materials*, McGraw-Hill, New York, 1963, p. 334.
- [15] B.J. Christensen, R.T. Coverdale, R.A. Olson, S.J. Ford, E.J. Garboczi, H.M. Jennings, T.O. Mason, *J. Am. Ceram. Soc.* 77 (1994) 2789.
- [16] B.A. Boukamp, *Equivalent Circuit (EQUIVCRT.PAS)*, Dept. of Chemical Tech., Univ. of Twente, P.O. Box 217, 7500 AE Enschede, Netherlands, 1988.

- [17] R.T. Coverdale, E.J. Garboczi, H.M. Jennings, B.J. Christensen, T.O. Mason, *J. Am. Ceram. Soc.* 76 (1993) 1513.
- [18] R.T. Coverdale, B.J. Christensen, T.O. Mason, H.M. Jennings, E.J. Garboczi, *J. Mater. Sci.* 29 (1994) 4984.
- [19] R.T. Coverdale, B.J. Christensen, T.O. Mason, H.M. Jennings, D.P. Bentz, E.J. Garboczi, *J. Mater. Sci.* 30 (1995) 712.
- [20] R.T. Coverdale, H.M. Jennings, E.J. Garboczi, *Comp. Mater. Sci.* 3 (1995) 465.
- [21] R.D. Cook, D.S. Malkus, M.E. Plesha, *Concepts and Applications of Finite Element Analysis*, Wiley, New York, 1989.
- [22] W.H. Press, B.P. Flannery, S.A. Teukolsky and W.T. Vetterlig, *Numerical Recipes: The Art of Scientific Computation (FORTRAN)* (Cambridge Univ. Press, Cambridge, 1989).
- [23] J.-H. Hwang, Ph.D. Dissertation, Northwestern University, Evanston, IL, 1996.